http://ansinet.com/itj

ITJ

ISSN 1812-5638

# INFORMATION TECHNOLOGY JOURNAL

ANSInet
Asian Network for Scientific Information
308 Lasani Town, Sargodha Road, Faisalabad - Pakistan

Information Technology Journal 9 (4): 782-789, 2010
ISSN 1812-5638


# Impulse Radio Ultra-Wide-Band Through Wall Imaging Radar Based on Multiple-Input Multiple-Output Antenna Arrays

H. Dong-Mei and Z. Qin-Yu
Shenzhen Graduate School, Harbin Institute of Technology, Shenzhen, 518055, China

**Abstract:** An Impulse Radio Ultra-Wide-Band (IR-UWB) Through Wall Imaging Radar (TWIR) employing linear MIMO antenna array, which is designed based on the effective array concept, is discussed in this study. An effective method to compute the signal travel time is also proposed. A major challenge of the IR-UWB TWIR is the cross-range resolution, which requires an antenna array with not only large operational bandwidth, but also certain aperture size. The real aperture array speeds up the data acquisition compared with Synthetic Aperture Radar (SAR), while it requires large number of elements and multiple channels in transceivers. To overcome this problem, Multiple-Input and Multiple-Output (MIMO) array is applied in the TWIR system. Effective array concept is used as the basis to design the MIMO array topology. Even though this concept is derived under narrow band far field condition firstly, it is demonstrated that it can be applied to the UWB near field TWIR. Performance of this MIMO array is investigated by TWIR image results. Numerical results showed that, the proposed MIMO array achieves the same resolution, lower side lobe level and lower artifacts, with much fewer antenna elements, as compared to the effective Single-Input and Multiple-Output (SIMO) array.

**Key words:** IR-UWB, Through Wall Imaging Radar (TWIR), Multiple-Input Multiple-Output (MIMO), effective array

## INTRODUCTION

Ultra-Wide-Band (UWB) systems have become one of the most important topics in research and industry worldwide. Large frequency bandwidth, precise ranging, penetrating ability are some salient features of UWB technique, which makes UWB be widely used in various imaging radar for different applications such as Ground Penetrating Radar (GPR) (Yarovoy *et al*., 2007a), medical imaging (Klemm *et al*., 2009) and Through Wall Imaging Radar (TWIR) (Lei and Ouyang, 2007b). Among all, through the wall surveillance is a difficult but important problem because of its perspective wide utilization, in such fields as, through wall imaging during security operation: e.g., to located hostages or terrorists and weapons behind walls, people trapped in a building during fire, persons buried under fallen walls after earthquake, border controls for detection of illegal immigrants, cigarettes in trucks, etc. Another wide area of utilization is detection, localization and tracking of the moving objects behind the wall. These technologies can save many lives during rescue operations, because rescue work will be safer and localization of the victims will be faster.

To identify the targets behind walls, the TWIR should possess high down-range and cross-range resolution. Since, the down-range resolution is purely determined by the operational bandwidth, which is an advantage of IR-UWB signals, one of the major challenges of the IR-UWB TWIR is the cross-range resolution, which required an antenna array with not only large operational bandwidth (Yarovoy *et al*., 2007b), but also certain aperture size. Such antenna array aperture can be either real or synthetic, or their combination. The Synthetic Aperture Radar (SAR) approach employs mechanical scanning usually with one transmit (Tx) and one receive (Rx) antennas. The scattered electromagnetic field is being spatially sampled in a dense regular grid, which makes data acquisition too slow (Daniels, 2004). The use of real aperture antenna array significantly speeds up the data acquisition. Such arrays have been developed for landmine detection and medical imaging (Yang *et al*., 2007). A more advanced GPR system combines SAR in on-track direction with a linear array in cross-track direction that receives the scattered field simultaneously with all antennas (Yarovoy *et al*., 2007a, b).

However, imaging antenna arrays with real aperture requires large number of elements and multiple channels in transceivers. To avoid unrealistic cost, electronics fabrication problems and large data flow for real-time imaging, the antenna array must be thinned. However,

**Corresponding Author:** Huang Dong-Mei, Room 208, Building C, HIT Campus of Shenzhen University Town, Shenzhen, Guangdong, 518055, China

aperture thinning generally causes the raise of side lobe level (Schwartz and Steinberg, 1998).

A good alternative array thinning can be Multiple-Input Multiple-Output (MIMO) approach. It is demonstrated by Schwartz and Steinberg (1998) and Lockwood and Foster (1994) that for a MIMO antenna array, the equivalent aperture is the spatial convolution of the transmitting antenna array aperture and the receiving antenna array aperture. As a result, the antenna array aperture size and element spacing of the effective array can be much larger and denser than those of the Single-Input Multiple-Output (SIMO) antenna array, providing better main lobe and side lobe control. The advantages of using MIMO antenna arrays are also demonstrated in (Haimovich *et al*., 2008; Savelyev *et al*., 2009). However, the effective array concept was derived by assuming far field radiation pattern. Whether, this concept works as you move closer to the array or away from the focal region for UWB is unknown. Lots of literatures for TWIR have put attention on the UWB imaging schemes (Lei and Ouyang, 2007a, b). However, work aiming at developing UWB-MIMO through wall radar is quite rare for the time being.

In this study, an IR-UWB through wall imaging radar, employing one dimension linear MIMO antenna array, is discussed. The topology of the MIMO array is designed based on the effective array concept in UWB beam forming. Even though this concept is derived from the far field, it is demonstrated it is can be applied in the near field as in TWIR. Performance of this MIMO array is investigated by the TWIR image results. The antenna arrays need not to be attached to the wall. The raw through wall radar data is generated using the Finite-Difference Time-Domain (FDTD) method. A two-dimension room with concrete walls, which is illuminated by IR-UWB pulse, is modeled inside the FDTD lattice. A conducting target is placed inside the room. The classical Back Projection (BP) algorithm was used to reconstruct the image of the target. The TWIR image of MIMO array is valuated by comparison with that of effective SIMO array.

## TWIR SYSTEM MODEL AND IMAGING TECHNIQUE

**TWIR system model:** For study of Through Wall Imaging Radar (TWIR), a two-dimension (2D) 2 m × 3 m room with concrete walls is modeled as shown in Fig. 1. The concrete walls are represented by their physical parameters, namely, a relative permittivity $\varepsilon_r$ = 7.0 and conductivity $\sigma = 5.0\times10^{-2}$ S m$^{-1}$. These values are chosen for an operating frequency f = 2 GHz. The wall is assumed to be homogeneous and frequency independent. The thickness of the wall is 10 cm. The target inside the room

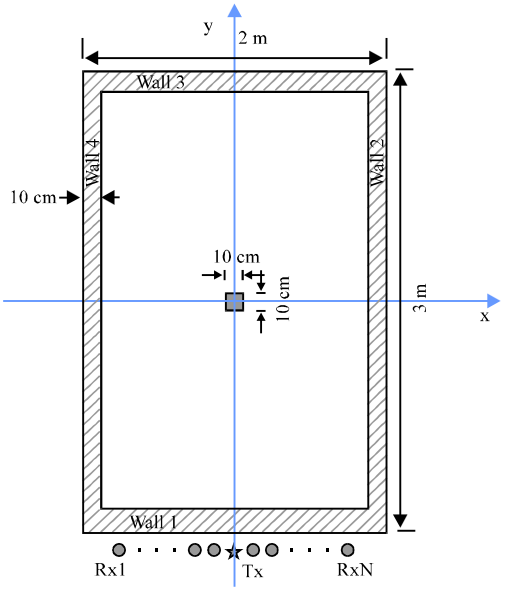


Fig. 1: TWIR measurement model configuration

consist of a 10 cm × 10 cm conducting box located at the center of the room, which is set to be the origin of the Cartesian coordinate system.

The transmitter and receivers are located outside the room, 0.5 cm from the wall 1 and are distributed along the side of the room in the x-direction. Assume that, the antenna elements are isotropic ideal point antennas and only one dimension linear array is considered here. The transmitter illuminates IR-UWB signal to the detecting or interesting area in room for active detection. The commonly used IR-UWB signal is the twice differentiated Gaussian pulse (Ries and Kaiser, 2006). Through wall imaging requires wave penetrating through specific building materials such as concrete blocks, clay bricks, drywall, asphalt shingles, fiberglass insulation etc. Data taken by Frazier (1998) have shown that most building materials are relatively transparent from 250 MHz to 3 GHz. Here, set time duration $\Delta T$ = 1 ns, leading to a -3 dB bandwidth from 0.9 to 2.5 GHz. The IR-UWB signal would be back-scattered, when it encounters the target, whose dielectric constant is different from air, the intensity of which is proportional to the electromagnetic reflectivity or scattering strength of the target. The back-scattered signals are received by the receive antenna array, which is composed of M transducers and the received data sequences are stored for post-processing.

**Imaging technique:** The imaging procedure is aimed to detect and reconstruct the image of the target from the stored data sequence. Assume that, the data is well pre-processed and calibrated in this study.

The imaging is based on time-domain back projection that has been widely applied to UWB radar imaging (Lei and Ouyang, 2007a). The idea is to correlate data collected at each antenna position as a function of round-trip delay time. The total round-trip delay time is the time to travel from the transmitter to the pixel and then back to a receiver. Back projection coherently sums the samples radar returns for each array element. What is meant by the phrase coherent summation is a process whereby the signal obtained at each array element position is time-shifted to match, or align, it to a particular pixel element in the image map. Following this, all the recorded amplitudes from each channel are added together on the spatial grid. At the target locations the signal amplitudes will add up coherently and should build up quickly.

Suppose, the back-scattered echo $y_{i,j}(t)$ is collected on the jth element in the linear receive antenna array, which is composed of M elements, when the ith transmit antenna illuminates the region of interest, which is composed of N elements. The back projected signal at pixel p in the image can be expressed mathematically as:

$$I(p) = \sum_{i=1}^{N}\sum_{j=1}^{M} w_{i,j}(p)\, y_{i,j}\left(t + \tau_{i,j}(p)\right)\Big|_{t=0} \quad (1)$$

where, $\tau_{i,j}(p)$ represents the propagation time from the ith transmit antenna to the point p and back to the jth receive antenna, which can be expressed as:

$$\tau_{i,j}(p) = \frac{R_{t,i}(p) + R_{r,j}(p)}{c}$$

where, $R_{t,i}(p)$ and $R_{r,j}(p)$ represents the propagation distance between the point p and the position of ith transmit and jth receive antennas, respectively. c denotes the propagation velocity in the medium. $w_{i,j}(p)$ is the weight coefficient which is designed to compensate the possible spherical radial spreading attenuation.

**Travel time estimation:** Through wall imaging requires wave penetrating through specific building materials, where various effects of the wall such as refraction and velocity change affect the imaging results. The time that a signal travels between the antennas and possible objects, which is critical in imaging algorithm, cannot be directly calculated like in homogeneous media. In general, the calculation of the travel time in multi-layered media is very time consuming and the time increases significantly when the number of layers increases. Hence, in most case before, the antenna arrays are placed attaching wall to simplify the problem to 2-layered media as shown in Fig. 2a. Assume that the wall is homogeneous and

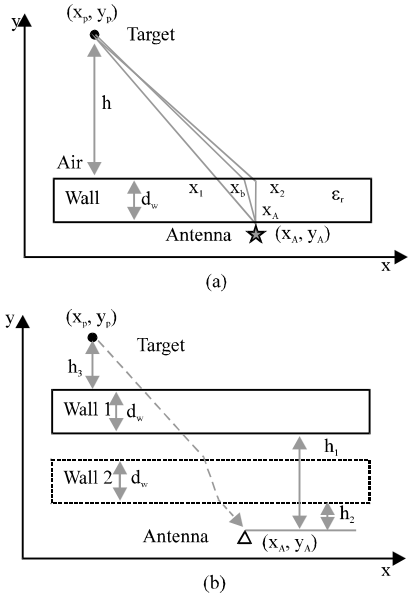


Fig. 2: Signal travel path in (a) 2-layered and (b) 3-layered media

frequency independent and the thickness of the wall $d_w$ and the dielectric constant $\varepsilon_r$ are known exactly. The approximation (Johansson and Mast, 1994) for the inflection point $x_b$ is:

$$x_b = x_2 + \sqrt{\frac{1}{\varepsilon_r}}(x_1 - x_2) = x_A + \frac{1}{\sqrt{\varepsilon_r}}\frac{d_w}{h + d_w}(x_p - x_A) \quad (2)$$

where, $x_2$ is the projection of antenna $(x_A, y_A)$ to the boundary, $x_1$ is the point at which the ray taking the straight path from antenna $(x_A, y_A)$ to target $(x_p, y_p)$, which penetrates the boundary. h is the vertical distance from the target to wall.

However, in practice, maintaining the antennas attaching walls is not always the case. The antennas often stand off walls from some distance, as shown in Fig. 2b, which corresponding the 3-layered media. In this study, a fast method for approximating it as in the case of 2-layered media is used. The idea was partly presented in Aftanas *et al.* (2008). In the case, relative permittivity of the air in front of wall and behind wall are the same, the incident angle of the incoming wave is the same as the angle of the outgoing wave which is leaving the wall. When distance between antenna and wall changes from $h_1$ to $h_2$, the true flight distance between antenna and target will not be changed, as shown in Fig. 2b. Now, all computations can be done with assumption that the rear side of the wall is at the antenna position and 2-layered model (wall-air), as shown in Fig. 2a, can be used, with $h = h_1 + h_3$. The virtual inflection point $x_b'$ can be given by:

$$x_b' = x_2' + \sqrt{\frac{1}{\varepsilon_r}}\left(x_1' - x_2'\right) = x_A + \frac{1}{\sqrt{\varepsilon_r}}\frac{d_w}{h_1 + h_3 + d_w}\left(x_p - x_A\right) \quad (3)$$

which can be used to compute the round-trip travel time, with significantly reduced computation complexity.

The accurate calculation of the total travel time can be computed like summation of both times, the time of flight in the air and the time of flight in the wall:

$$\tau(p) = \frac{R_A}{c} + \frac{R_W}{v_w} \quad (4)$$

where, $R_A$ and $R_W$ represent the travel distance in air and wall, respectively. The velocity in the wall is given by

$$v_w = \frac{c}{\sqrt{\varepsilon_r}}$$

## DESIGN OF THE MIMO ANTENNA ARRAY

In the UWB radar systems, the cross-range resolution and the side lobe level are strongly related to the antenna topology. Larger array aperture gives finer cross-range resolution while denser element spacing gives lower side lobe level. Hence, to have fine cross-range resolution and low side lobe, large antenna array with dense element spacing is required. To overcome high complexity and associated high system costs, we adapt the concept of Multiple Input and Multiple Output (MIMO) antenna array to achieve both fine cross-range resolution and low side lobe level with a fewer number of elements instead of the conventional Single Input and Multiple Output (SIMO) array.

The effective array concept is used as the basis of designing MIMO antenna array from SIMO antenna array. The effective array is a one-way linear array having the same response as the pulse-echo (or two-way) response from transmit and receive arrays. In narrowband (NB), the radiation pattern of effective array is equivalent to the multiplication of transmit and receive patterns. Therefore the effective array is the spatial convolution of transmit and receive arrays (Lockwood and Foster, 1994). That is, the effective SIMO antenna aperture E(x) can be written as:

$$E(x) = a_{Tx}(x) * a_{Rx}(x) \quad (5)$$

where, $a_{Tx}(x)$ is the transmitting array aperture and $a_{Rx}(x)$ is the receiving array aperture, x represents the location of the element in the antenna array and * denotes spatial convolution.

However, it is not the case in UWB (Schwartz and Steinberg, 1998). A simple scattering medium consisting

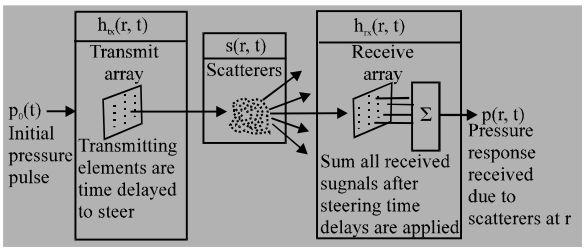


Fig. 3: The pulse-echo linear system

of rigid, point scatters is assumed. The pulse-echo process is modeled as a linear system (Fig. 3) with a well-defined Point Spread Function (PSF):

$$p(r, t) = p_0(t) * h_{Tx}(r, t) * s(r,t) * h_{Rx}(r, t) = PSF * s(r,t) \quad (6)$$

where, r is the location vector of the scatters. $p_0(t)$ is the transmitted UWB pulse, $h_{Tx}(r, t)$ and $h_{Rx}(r, t)$ is the Tx array and Rx array response, respectively, s(r,t) is the impulse response of the scatters.

In the far field, the antenna array response is not only the function of angle $\theta$, but also of time t. PSF for UWB systems for a scatter at bore sight and at a distance $r_0$ for N-element linear transmit and receive arrays are (Schwartz and Steinberg, 1998):

$$PSF_{UWB} = p_0(t) * h_{Tx}(t, \theta) * h_{Rx}(t, \theta) \quad (7)$$

Where:

$$h(t, \theta) = \sum_{i=1}^{N} A(x_i)\frac{\delta\left(t - \frac{x_i \sin\theta}{c}\right)}{2\pi r_0} \quad (8)$$

The UWB waveform in the Interference Region (IR), where, $\sin\theta \le c\Delta T/d$, can be described by NB theory. However, in the Non-Interference Region (NIR), the NB theory breaks down. The NIR beam pattern results from a convolution in time of transmit and receive impulse responses. Consequently, the radiation pattern of UWB effective array is not simply equivalent to the multiplication of transmit and receive array patterns, as in narrowband (NB). From Eq. 7, the UWB effective array is seen to be the array that produces the space-time impulse response $h_{eff}(t,\theta)$ equal to the convolution of transmit and receive space-time impulse responses. For uniformly tapered, linear transmit and receive arrays, $h_{eff}(t,\theta)$ is:

$$\begin{aligned} h_{eff}(t, \theta) &= h_{Tx}(t, \theta) *_t h_{Rx}(t, \theta) \\ &= \sum_{i=1}^{N_{Tx}} \delta\left(t - \frac{x_{Tx}^i \sin\theta}{c}\right) *_t \sum_{j=1}^{N_{Rx}} \delta\left(t - \frac{x_{Rx}^j \sin\theta}{c}\right) \end{aligned} \quad (9)$$

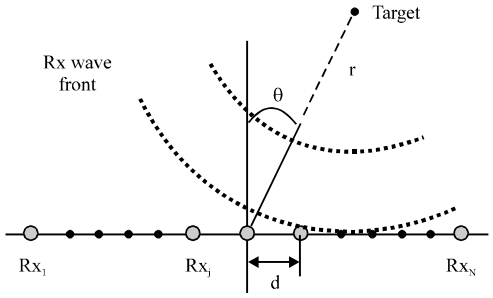


Fig. 4: Near field beam forming scheme

At sin θ = 1 (array axis), the temporal spacing between pulses directly corresponds to element spacing in the array. Therefore, the effective array is found by viewing $h_{eff}(t, \theta)$ along the array axis:

$$\begin{aligned} h_{eff}(t,\sin\theta=1) &= \sum_{i=1}^{N_{Tx}} \delta\left(t-\frac{x_{Tx}^{i}}{c}\right) *_{t} \sum_{j=1}^{N_{Rx}} \delta\left(t-\frac{x_{Rx}^{j}}{c}\right) \\ \Rightarrow w_{eff}(x) &= \sum_{i=1}^{N_{Tx}} \delta\left(x-x_{Tx}^{i}\right) *_{x} \sum_{j=1}^{N_{Rx}} \delta\left(x-x_{Rx}^{j}\right) \end{aligned} \quad (10)$$

Thus, the UWB effective array is also shown to be a spatial convolution of transmit and receive arrays.

In the near field, the wave front received by the array is not a planar wave front as in the far field, but a spherical wave front, as shown in Fig. 4. The antenna array response is not only the function of angle θ, time t, but also the range of the target $r_0$, through the delay time and the amplitude. Assume that, the amplitudes attenuation, affecting by the radial spherical spreading, are completely compensated. The UWB near field antenna array impulse response $h_N(t, \theta, r_0)$ can be expressed as:

$$h_N(t,\theta,r_0) = \sum_{i=1}^{N} \delta\left(t+\frac{\sqrt{r_0^2+x_i^2-2\sin\theta r_0 x_i}-r_0}{c}\right) \quad (11)$$

The pulse-echo impulse response of UWB near-field array $h_{eff-N}(t,\theta,r_0)$ is:

$$\begin{aligned} h_{eff-N}(t,\theta,r_0) &= h_{Tx-N}(t,\theta,r_0) *_{t} h_{Rx-N}(t,\theta,r_0) \\ &= \sum_{i=1}^{N_{Tx}} \delta\left(t+\left(\sqrt{r_0^2+\left(x_{Tx}^{i}\right)^2-2\sin\theta r_0 x_{Tx}^{i}}-r_0\right)/c\right) \\ &*_{t} \sum_{j=1}^{N_{Rx}} \delta\left(t+\left(\sqrt{r_0^2+\left(x_{Rx}^{j}\right)^2-2\sin\theta r_0 x_{Rx}^{j}}-r_0\right)/c\right) \end{aligned} \quad (12)$$

The effective array also can be found by viewing $h_{eff-N}(t,\theta,r_0)$ along the array axis at sin θ = 1:

$$\begin{aligned} h_{eff-N}(t,\sin\theta=1,r_0) &= \sum_{i=1}^{N_{Tx}} \delta\left(t-\frac{x_{Tx}^{i}}{c}\right) *_{t} \sum_{j=1}^{N_{Rx}} \delta\left(t-\frac{x_{Rx}^{j}}{c}\right) \\ \Rightarrow w_{eff-N}(x) &= \sum_{i=1}^{N_{Tx}} \delta\left(x-x_{Tx}^{i}\right) *_{x} \sum_{j=1}^{N_{Rx}} \delta\left(x-x_{Rx}^{j}\right) \end{aligned} \quad (13)$$

It is shown that, the UWB effective array in the near field is also a spatial convolution of transmit and receive arrays. This forms the basis of the method we have developed for designing MIMO arrays in TWIR. From SIMO array, we can search for possible transmit and receive elements positions of the MIMO array, which gives the corresponding effective SIMO array.

In the UWB system, a desired one-dimension effective array will be rectangular, which means uniformly weighted, dense periodic linear array with $\lambda_{min}/2$ element spacing (Ries and Kaiser, 2006; Kaiser *et al*., 2009; Schwartz and Steinberg, 1998), where $\lambda_{min}$ is the wavelength corresponding to the -3 dB high frequency. Many different strategies can be used to obtain MIMO arrays (Schwartz and Steinberg, 1998), such as Triangularly Spatial-Tapered (TST) and Interpolation (INT) method. For this desired rectangular array, the rectangular interpolation is preferred. The transmit and receive element spacing that form the interpolation array are:

$$d_{Rx} = L_{Tx} + d_{Tx} \quad (14)$$

$L_{tx}$ = transmitting array length, $d_{Rx}$ receive array periodicity and $d_{Tx}$ = transmit array periodicity. The number of elements in MIMO transmit array $N_{Tx}$, receive array $N_{Rx}$ and SIMO effective array M are:

$$M = N_{Tx} \times N_{Rx} \quad (15)$$

With proper designing, the number of antenna elements can be reduced to $2\sqrt{M}$, which reduced the cost and complexity dramatically, especially for large array case.

## SIMULATION AND RESULTS

Here, simulated data of IR-UWB radar in front of a concrete room had been generated by the Finite-Difference Time-Domain (FDTD) numerical method, for the through-wall imaging study. The room as shown in Fig. 1 was considered. The FDTD spatial and temporal resolution parameters used in the modeling and simulation were set as follows: spatial resolution dx =dy = 0.63 cm; time resolution dt = 10.5 ps. The whole computational domain of FDTD was truncated using the Perfectly Matched Layer (PML) (Taflove and Hagness, 2000) absorbing boundary conditions.

For SIMO, one transmitter and 25 elements dense linear receive array were considered as shown in Fig. 5a, with pentacle representing the transmitter and circ the receive antenna. The center of transmit and receive array

located at (0, -1.55), adjacent element distance $d = \lambda_{min}/2 = 6.3$ cm and the aperture length L = 151.2 cm. The conducting box was in the near field of the SIMO array. The MIMO array was designed based on the effective array concept using the above SIMO array as the desired effective array. The antenna array consisted of 5 elements transmit array and 5 elements receive array as shown in Fig. 5b, with adjacent elements distance $d_{Tx}$ = 6.3 cm, $d_{Rx}$ = 31.5 cm, respectively. Compared with SIMO, the number of antenna elements employed here in the MIMO had been reduced by 2.6 times.

The received raw signals included the direct signal from the transmit antenna and echoes from both the concrete room and the box. For this case, the direct signal from the transmit antenna, being much stronger than the other echoes, made it difficult to see the smaller signals such as the box echoes. In order to better display the radar images of the targets, the isolated targets responses were obtained by subtracting the received signals of the empty room from the received signals of the room with targets. This process removed the stationary clutter and kept only changes inside the room.

Figure 6-8 showed the radar images and detected image of the box inside the room reconstructed by the BP algorithm, with SIMO and MIMO antenna array, respectively. Here, a logarithmic scale had been used to better display images of the targets. In addition, for clarity, a detected image was derived by setting a threshold level (equal to -10 dB) in the plotting program to suppress the side lobes of the generated images and display only the peak magnitudes. The practical location of box was also shown in images as yellow squares.

As shown in Fig. 6 and 7, both SIMO and MIMO could detect the target and located the target correctly with about the same resolution, while, the side lobe level in the MIMO image was lower than that in SIMO image. In TWIR images, there were some artifacts in the image, which were caused by the multiple reflections in wall or between walls. Some of these artifacts were stronger than the side lobe level of the target and would be visible in detected image, as shown in Fig. 6 for SIMO, leading to error in following identification. From Fig. 7, it could be observed that, the level of artifacts in MIMO image was lower than that of SIMO, leading to no artifacts in the detected image by threshold of -10 dB. The MIMO array

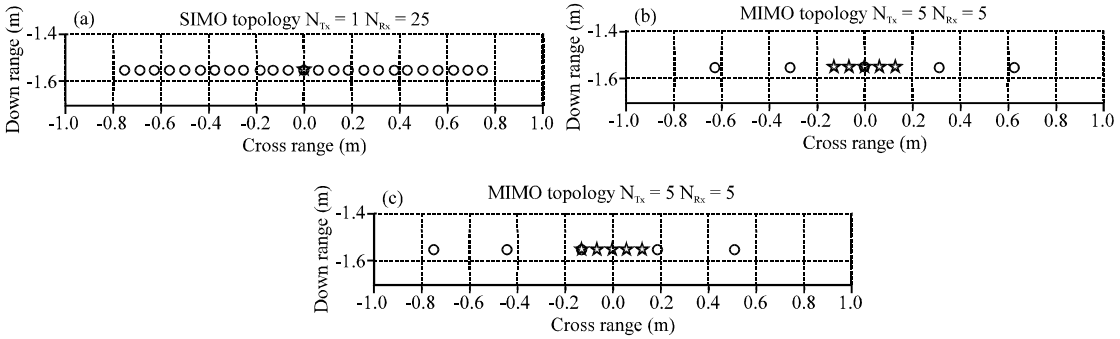


Fig. 5: Array topology of (a) SIMO, (b) MIMO, (c) MIMO with deviated center

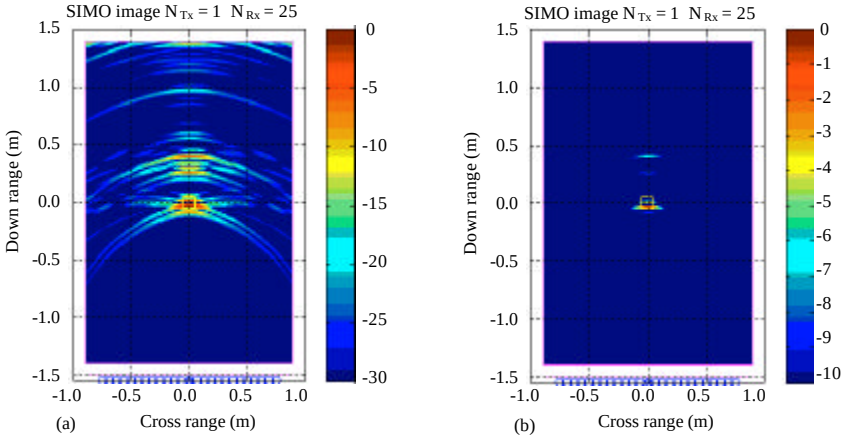


Fig. 6: The (a) radar image and (b) detected image from SIMO

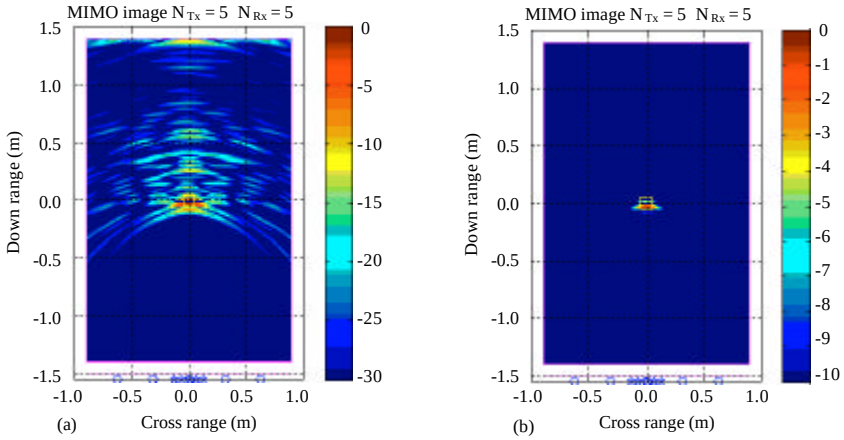


Fig. 7: The (a) radar image and (b) detected image from MIMO

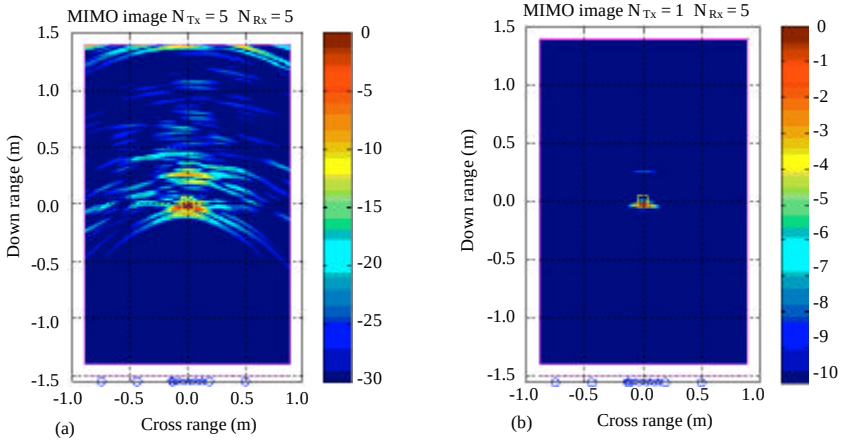


Fig. 8: The (a) radar and (b) detected image from MIMO with deviated center

topology redistributed the effects of walls into other region in the time-space (or range-cross range) plane.

Figure 8 showed images from MIMO array as shown in Fig. 5c. The parameters of this array was the same as that in Fig. 5b, except the center of the receive array deviating about -12.6 cm from the center of the transmit array, which was the same as in Fig. 5b. In this case, the level of the artifacts increased, as compared with images in Fig. 7, which caused an artifact in the detected image. However, the level was still lower than that of SIMO array. The co-center characteristic of the MIMO array related to better performance of image.

## CONCLUSIONS

In this study, the IR-UWB through wall imaging radar employing one dimension linear MIMO antenna array, which is designed based on the effective array concept, is discussed. Even though this concept is derived under narrow band far field condition firstly, it is demonstrated that it can be applied to the UWB near field TWIR. The antenna arrays do not need to be attached to the wall as before. The radar and detected image of the MIMO array have been compared with that of the effective SIMO array. Results show that, the designed MIMO array works very well. The resolution of the MIMO and the SIMO is nearly the same; the side lobe level of MIMO is lower than that of the SIMO. Moreover, the MIMO array leads to lower artifacts level in radar images even though the center of the transmit and receive array is not the same and no artifact in detected image by threshold of -10dB, when the centers is the same. The number of antenna elements in MIMO is much fewer than that in SIMO, especially for large array. This property is very perspective in the TWIR to reduce corresponding cost and complexity. The further investigation will include multiple targets and moving targets.

**ACKNOWLEDGMENTS**

This research is supported by the National Nature Science Foundation of China under Grant No. 60702034. The author would like to thank Ms. B.L. Liu for her assistance in this work, Mr. Ting-ting Zhang and Ms. Jing Meng for their revising this study.

**REFERENCES**

Aftanas, M., J. Rovòáková, M. Drutarovsky and D. Kocur, 2008. Efficient method of TOA estimation for through wall imaging by UWB radar. Proceedings of IEEE ICUWB, Sept. 10-12, Leibniz Universitat Hannover, Germany, pp: 101-104.

Daniels, D.J., 2004. Ground Penetrating Radar. 2nd Edn., The Institution of Electrical Engineers, London, ISBN-10: 0-86341-360-9.

Frazier, L., 1998. MDR for law enforcement. IEEE Potentials, 16: 23-26.

Haimovich, A.M., R.S. Blum and L.J. Cimini, 2008. MIMO radar with widely separated antennas. IEEE Signal Proces. Mag., 25: 116-129.

Johansson, E.M. and J.E. Mast, 1994. Three-dimensional ground penetrating radar imaging using synthetic aperture time-domain focusing. Proceedings of SPIE Conference on Advanced Microwave and Millimeter Wave Detectors, Sept. 14, SPIE, USA., pp: 205-214.

Kaiser, T., F. Zheng and E. Dimitrov, 2009. An overview of ultra-wide-band systems with MIMO. Proc. IEEE., 97: 285-312.

Klemm, M., I.J. Craddock, J.A. Leendertz, A. Preece and R. Benjamin, 2009. Radar-based breast cancer detection using a hemispherical antenna array-experimental results. IEEE Trans. Antennas Propag., 57: 1692-1704.

Lei, C. and S. Ouyang, 2007a. Through-wall surveillance using ultra-wideb and short pulse radar: Numerical simulation. Proceedings of 2nd IEEE Conference on Industrial Electronics and Applications, May 23-25, Harbin, China, pp: 1551-1554.

Lei, C. and S. Ouyang, 2007b. A time-domain beamformer for UWB through-wall imaging. Proceedings of IEEE, Oct. 30-Nov. 2, Taipei, Taiwan, pp: 1-4.

Lockwood, G.R. and F.S. Foster, 1994. Optimizing sparse two-dimensional transducer arrays using an effective aperture approach. Proceedings of Ultrasonics Symposium, Nov. 1-4, Cannes, pp: 1497-1501.

Ries, S. and T. Kaiser, 2006. Ultra wideband impulse beamforming: It is a different world. Signal Proces., 86: 2198-2207.

Savelyev, T.G., X. Zhuge, A.G. Yarovoy, L.P. Ligthart and B. Levitas, 2009. Comparison of UWB SAR and MIMO-based short-range imaging radars. Proceedings of the 6th European Radar Conference, Sept. 30-Oct. 2, Rome, Italy, pp: 109-112.

Schwartz, J.L. and B.D. Steinberg, 1998. Ultrasparse, ultrawideband arrays. IEEE Trans. Ultrasonics, Ferroelectrics Frequency Control, 45: 376-393.

Taflove, A. and S.C. Hagness, 2000. Computational Electrodynamics: The Finite-Difference Time-Domain Method. Artech House, Norwood, Manchester.

Yang, B., A.G. Yarovoy and L.P. Ligthart, 2007. Performance analysis of UWB antenna array for short-range imaging. Proceedings of EuCAP, Nov. 11-16, Edinburgh, UK, pp: 1-6.

Yarovoy, A.G., T.G. Savelyev, P.J. Aubry, P.E. Lys and L.P. Ligthart, 2007a. UWB array-based sensor for near-field imaging. IEEE Trans. MTT, 55: 1288-1295.

Yarovoy, A.G., X. Zhuge, T.G. Savelyev and L.P. Ligthart, 2007b. Comparison of UWB technologies for human being detection with radar. Proceedings of the 4th European Radar Conference, Oct. 10-12, Munich, Germany, pp: 295-298.